Mon. Not. R. Astron. Soc. **000**, 1–9 () Printed 1 September 2016 (MN LATEX style file v2.2)

H, He-like recombination spectra II: *l*-changing collisions for He Rydberg states

F. Guzmán[1], N. R. Badnell[2], R. J. R. Williams[3], P. A. M. van Hoof[4], M. Chatzikos[1] and G. J. Ferland[1].
[1]Department of Physics and Astronomy, University of Kentucky, Lexington, KY 40506, USA
[2]Department of Physics, University of Strathclyde, Glasgow G4 0NG, UK
[3]AWE plc, Aldermaston, Reading RG7 4PR, UK
[4]Royal Observatory of Belgium, Ringlaan 3, 1180 Brussels, Belgium

Received

arXiv:1608.08947v1 [astro-ph.CO] 31 Aug 2016

ABSTRACT

Cosmological models can be constrained by determining primordial abundances. Accurate predictions of the He I spectrum are needed to determine the primordial helium abundance to a precision of $< 1\%$ in order to constrain Big Bang Nucleosynthesis models. Theoretical line emissivities at least this accurate are needed if this precision is to be achieved. In the first paper of this series, which focused on H I, we showed that differences in *l*-changing collisional rate coefficients predicted by three different theories can translate into 10% changes in predictions for H I spectra. Here we consider the more complicated case of He atoms, where low-*l* subshells are not energy degenerate. A criterion for deciding when the energy separation between *l* subshells is small enough to apply energy-degenerate collisional theories is given. Moreover, for certain conditions, the Bethe approximation originally proposed by Pengelly & Seaton (1964) is not sufficiently accurate. We introduce a simple modification of this theory which leads to rate coefficients which agree well with those obtained from pure quantal calculations using the approach of Vrinceanu et al. (2012). We show that the *l*-changing rate coefficients from the different theoretical approaches lead to differences of $\sim 10\%$ in He I emissivities in simulations of H II regions using spectral code Cloudy.

Key words: atomic data – ISM: abundances – (ISM:) HII regions – cosmology: observations – (cosmology:) primordial nucleosynthesis

1 INTRODUCTION

Measurement of the primordial helium abundance relies on the observation of H I and He I recombination lines in low-metallicity extragalactic H II regions (Izotov et al. 2007). The statistical uncertainties in derived He abundances must be less than 1% (Olive et al. 2000) if they are to test Standard Big Bang Nucleosynthesis (SBBN) models (Izotov et al. 2014). This high precision must be supported by the fundamental atomic data employed in the H I and He I emissivity predictions.

In the first paper of this series (Guzmán et al. 2016), hereafter P1, we examined how dipole *l*-changing collisions influence the H I spectrum. New semi-classical (SC) rate coefficients from Vrinceanu et al. (2012) (hereafter VOS12) are about an order of magnitude smaller than those obtained using the long-standard theory of Pengelly & Seaton (1964) (hereafter PS64). The quantum mechanical (QM) treatment by Vrinceanu & Flannery (2001a) is in good agreement with PS64. The dipole collision probabilities of the PS64 and QM theories are divergent, with the cross section tending to infinity for collisions with very distant particles. This necessitates the imposition of a cut-off at large impact parameters, which in turn creates an additional uncertainty. The standard approach is to consider physical criteria such as collective effects (Debye screening) and the lifetime of the state to set this cut-off (see PS64). P1 discussed the possible cut-offs that can be employed, and compared H I emission spectra for each. The uncertainties imposed by the cut-offs are in addition to the differences with the SC approaches in the cross sections. Overall, we showed that the rate coefficients obtained from QM vs SC theories result in differences of up to 10% for H I recombination line spectra. We recommended that PS64 be used for dipole transitions because of its speed of evaluation and good agreement with the QM results of Vrinceanu & Flannery (2001a).

This paper re-examines the theory of *l*-changing collisions for the more complex and important case of He I Rydberg states. In the case of H-like systems we deal with only one electron and all *l* subshells can be taken to be energy degenerate. The He I case presents a richer phenomenology with its two spin systems where large-*l* subshells are nearly degenerate, while small-*l* subshells are non-degenerate. Different approaches are needed to treat collisions for each of these cases. The degenerate and non-degenerate treatments

© RAS

are reviewed in Section 2. In Section 2.3, we introduce a modification to the PS64 approach at small impact parameters, guided by the VOS12-QM probabilities, which gives improved accuracy in circumstances sensitive to close collisions, i.e. low temperatures and/or high densities. In Section 3, we test the influence of our results on the final spectrum by calculating He I recombination emissivities for different densities using Cloudy, the spectral simulation code last described by Ferland et al. (2013). We recommend the best rates to be used in simulations and abundance determinations, and present comparisons of the He I lines obtained using different data, in Section 3.2.

2 ATOMIC PHYSICS OF *l*-CHANGING COLLISIONS

We focus on l-changing collisions within the same n-shell. These can be caused by electron collisions or by the angular momentum Stark-mixing created by a slow-moving heavy charged-particle such as a proton or helium nucleus. Electron collisions (energy changing) dominate transitions between non-degenerate l-subshells (Brocklehurst 1972). Heavy particles will dominate when there is little or no energy exchange and they are effective at small impact velocities and large distances. This requires the l-subshells to be energy degenerate, or nearly so.

Different approaches must be adopted for different l-subshells in He. Unlike the H case, LS-coupling in He gives rise to non-degenerate l-subshells. Although large-l states may be nearly degenerate in energy, smaller ones ($l < 3$) are highly non-degenerate. Moreover, energy degenerate l-changing collision theories overestimate rate coefficients when applied to non-degenerate transitions. In this ($l < 3$) case the Seaton (1962) formalism (S62) is used and adapted to proton collisions (Benjamin et al. 1999; Porter et al. 2009). Larger l are 'nearly degenerate' so it is necessary to review the QM cut-off criteria adopted in P1 for degenerate l-subshells. This is analyzed in Section 2.2.

We have considered the competing theories for energy degenerate collisions discussed in P1. As with H, their predicted collisional rate coefficients for He do not agree with each other. These are shown in Fig. 1, where, as in the H case, the original calculations from PS64 agree with VOS12 QM calculations (see Section 2.1 for details). Both are larger than the SC data given by the same authors.

2.1 *l*-changing collision approaches

In l-changing collisions between heavy charged-particles and an atom, the angular momentum of the electron within an n-shell is changed by the Stark effect caused by the electric field of the distant slow-moving particle (typically a proton or an alpha particle) so that $nl \rightarrow nl'$. These collisions redistribute l-subshell populations after recombination and can affect how electrons cascade to ground, changing the line emissivities. In P1 we showed that the use of different l-changing data led to differences in the final emissivities in H I of up to 10%, especially for transitions from high n to low n .

In this paper we use the following notation for the various theories. The impact parameter Bethe-Born approximation of Pengelly & Seaton (1964) is called PS64. New QM and SC treatments were proposed by Vrinceanu & Flannery (2001a,b). Following the nomenclature from P1, we refer to these theories as VOS12-QM and VOS12-SC respectively[1]. The latter was further simplified in Vrinceanu et al. (2012) by approximating the scaled angular momentum, l/n, as a continuous variable in order to provide a simple analytic equation for rate coefficients. We denote this method VOS12-SSC (where SSC stands for Simplified Semi-Classical). These theories produce very different results. SC rate coefficients are smaller than VOS12-QM and PS64 by a factor of ~ 6 while the last two are in good agreement.

Two issues affect our choice of methods. First, the probabilities predicted by QM methods are divergent for dipole ($\Delta l = 1$) transitions at large impact parameter. A cut-off based on physical collective effects was chosen to truncate the probability integral. The SC treatment does not have this problem but it fails to describe long-range probabilities which QM methods do describe, making them smaller than the QM cross sections. We note that all of our H- and He-like recombination predictions in the series of papers culminating in Porter et al. (2012) were based on VOS12-SC from Vrinceanu & Flannery (2001a), while previous work by the UCL group, culminating in Storey & Hummer (1995), used PS64.

2.2 Cut-offs for non-degenerate levels at large impact parameters

Two cut-offs were proposed by PS64 and discussed in P1. The first is:

$$R_{\rm c}^{d} = 0.72 v \tau \,, \tag{1}$$

with v being the projectile speed and τ the lifetime of the initial state. This is motivated by that fact that the initial state must not radiate before the collision is complete. The second possible cut-off is the Debye screening length,

$$R_{\rm D} = \left[\frac{k_{\rm B} T_e}{4\pi e^2 n_e} \right]^{1/2} , \tag{2}$$

where e is the electron charge, $k_{\rm B}$ is the Boltzmann constant, T_e is the electron temperature and n_e is the electron density. The smallest of these cut-offs sets the maximum impact parameter for which the collision can occur.

If the energy difference between the initial and final states is large compared with the line-widths, $\hbar/\tau$, PS64 replace equation (1) by an energy dependent cut-off:

$$R_{\rm c}^{nd} = 1.12 \hbar v / \Delta E \,. \tag{3}$$

The question of where the non-degeneracy is large enough to apply equation (3) is summarized in Fig.1. For $l \geqslant 3$ Brocklehurst (1972) proposed using the following inequality to select those l-changing collisions where PS64 cut-offs for degenerate transitions of equations (1) and (2) can be applied:

$$\beta = \frac{L \Delta E}{\hbar 2 W} < 0.4 \,. \tag{4}$$

In equation (4), L and W are the mean angular momentum and energy of the projectile. This implies that the collision time should be less than forty per cent of the spontaneous transition time. This is usually fulfilled for $l > 7$.

Fig. 1 compares different l-changing collision rate coefficients for H^++He ($n = 30; l \rightarrow l' = l - 1$). The vertical lines indicate

[1] This notation comes about because these formalisms are summarized in Vrinceanu et al. (2012) who also give computationally convenient expressions.

the l'-ranges where the different collision theories apply. The first range ($l' = 0-2$) is where l-changing collisions by electrons dominate. The next range ($l' = 3-6$) covers those l' where equation (4) is not satisfied and the l-subshells are non-degenerate, but l-changing proton collisions dominate over electron ones. In the final range ($l' = 7-28$) the inequality (4) is satisfied. Finally, the thick blue vertical bar beyond $l' = 13$ shows the l' from where the PS64 rates, using both the degeneracy cut-off from eq (3) and the non-degenerate cut-off from equation (1) give the same result. For lower l, $R_c^{nd} < R_c^d$ and for higher l, $R_c^d \leqslant R_c^{nd}$. Using the non-degenerate cut-off for $l' \leqslant 13$ and the degenerate one for $l' > 13$ ensures a smooth merging of the results. For this reason, we decided to use the latter as a criterion to separate degenerate and nearly degenerate subshells. In our calculations we use the QM methods with the minimum of the cut-offs from equations (1), (2) and (3) when $l \geqslant 3$:

$$R_c = \min\{R_c^d, R_c^{nd}, R_D\}\,. \tag{5}$$

If $l < 3$, the energy splitting is large enough for electron collisions to dominate. Electron-impact collisions have been calculated using the S62 impact parameter method (blue line in Fig. 1) and are clearly larger than the non-degenerate QM proton impact rate coefficients. For $l \geqslant 3$, l subshells are much closer in energy and $\Delta E \to 0$ as $l \to \infty$. Note that the SC results are comparable to electron collisional ones even at this high n shell ($n = 30$), as shown in Fig. 1. For the non-degenerate l subshells ($l < 3$), we use the adapted S62 method to derive proton collisional rate coefficients (solid black line in Fig. 1). This guarantees that the l -changing collisional rate is a smooth function of l where collision are primarily driven by electrons for $l < 3$ and then by protons for high l (see Fig. 1).

Our criterion differs from the one employed by Benjamin et al. (1999), where the S62 method was used for low l until it was within 6% of the PS64 degenerate l-changing collisional rates. We found that, at high n, this never occurs, as seen in Fig. 1.

2.3 Modified Pengelly and Seaton (PS-M)

Pengelly & Seaton (1964) used the impact parameter method to describe the cross section, σ_{ji}, for the transition $i \to j$

$$\sigma_{ji} = 2\pi \int_0^\infty P_{ji}(R) R \mathrm{d}R\,, \tag{6}$$

in terms of the probability P_{ji} and impact parameter R.

On restricting to dipole transitions ($l \to l' = l \pm 1$), they made use of the Bethe form of the Born approximation for P:

$$P_{ji}(R) = \frac{4Z_p^2}{3v^2\omega_i}\frac{S_{ji}}{R^2}\,, \tag{7}$$

where S_{ji} is the atomic line strength, ω_i the statistical weight of the initial state i, and Z_p and v are the projectile charge and velocity, respectively. Omitting the spin statistical weight from S_{ji}, then $\omega_i \to \omega_l = (2l+1)$.

This approach gives rise to divergent cross sections as $R \to 0$ and $R \to \infty$. Treatments to cut-off the probability at large impact parameters (R_c) were discussed in Section 2.2. PS64 introduced a cut-off, R_1, at small impact parameters defined by requiring continuity with an upper bound to the transition probability of

$$P = \frac{1}{2} \qquad \text{for} \qquad R \leqslant R_1\,, \tag{8}$$

where they assumed that in reality the probability for $R < R_1$ followed a rapidly oscillating Born-like $\sim \sin^2$ behaviour, but that it was sufficiently accurate to represent the mean behaviour when determining the overall collision cross section. Initially, PS64 took $P = P_{ji}$ but in deriving their formula (43) they took $P = \sum_{j\neq i} P_{ji}$.

The detailed QM results of Vrinceanu & Flannery (2001a) — see Fig. 2 — do indeed show that the transition probability saturates at some R, and undergoes oscillations as R reduces further. However, for $n > 1$ the envelope of the probability oscillations decreases as R becomes smaller, rather than remaining constant as assumed by PS64. This suggests the following modification for $R \leqslant R_1 \leqslant R_c$:

$$P(R) = P_1 \frac{R}{R_1}\,, \tag{9}$$

where

$$2P_1 R_1^2 = \frac{8Z_p^2 \mu I_H}{3E\omega_l} S_{ji}\,, \tag{10}$$

and μ is the reduced mass, E the energy in the centre-of-mass reference frame, and I_H is the Rydberg energy. Fig. 2 shows that this choice of probability better matches the QM probability in the range $b/n^2 = 10-100$, and to which low temperature rate coefficients are sensitive.

Now, define E_{min} to be the energy at which $R_1 = R_c$. Then, for $E \geqslant E_{min}$, we have

$$\sigma_{ji} = \frac{\pi a_0^2 \mu I_H}{2\omega_l E} D_{ji}\left[\frac{2}{3} + 2\log\left(\frac{R_c}{R_1}\right)\right]. \tag{11}$$

Here a_0 is the Bohr radius. The factor $\frac{2}{3}$ in (11) arises from the linear form of (9) and taking $P_1 = \frac{1}{2}$ and summing-over j in (10) regains the original PS64 formula (for a constant P). Note, PS64 consider an unresolved $l \to l \pm 1$ cross section, i.e. summed-over final l'. We discuss historic modifications of the original PS64 formula to obtain a final-state resolved form, and the lack of reciprocity that the use of an R_1 engenders, in Appendix A.

Writing

$$D_{ji} = \frac{8Z_p^2}{3a_0^2} S_{ji}, \tag{12}$$

we have

$$D_{nl\to nl'} = \left(\frac{Z_p}{Z_t}\right)^2 6n^2 l_> \left(n^2 - l_>^2\right), \tag{13}$$

where Z_t is the target charge and $l_> = \max(l, l')$ and $l' = l \pm 1$ still.

The rate coefficient q_{ji} is obtained by convolving the cross section with a Maxwellian energy distribution. The lifetime or energy splitting cut-off ($R_c = \min(R_c^d, R_c^{nd})$) depends on the scattering energy ($R_c \propto \sqrt{E}$) while the Debye limit ($R_c = R_D$) is independent of it. PS64 assumed a mean cut-off by using one or the other at all energies, based-on the smallest at $3v_{RMS}/4$ for example. Quadrature of the QM cross sections simply switches between the two forms as appropriate. We can implement the same approach analytically by splitting the convolution integral into two parts: define E_c be the energy such that $R_D = \min(R_c^d, R_c^{nd})$, then

$$q_{ji} = \frac{a_0^3}{\tau_0\omega_l}\left(\frac{\pi\mu I_H}{k_B T}\right)^{\frac{1}{2}} D_{ji}\left[\frac{2}{3}\mathrm{e}^{-\overline{U}_m} + 2E_1(\overline{U}_m) - E_1(U_c)\right], \tag{14}$$

where $\overline{U}_m^2 = U_m U_c$, $U_m = ER_1^2/(R_c^2 k_B T) = E_{min}(\text{Debye})/k_B T$, $U_c = E_c/k_B T$, E_1 is the first exponential integral and $\tau_0 = \hbar/I_H = 2.4188 \times 10^{-17}$ s is the atomic unit of time. Note, taking $\overline{U}_m =$

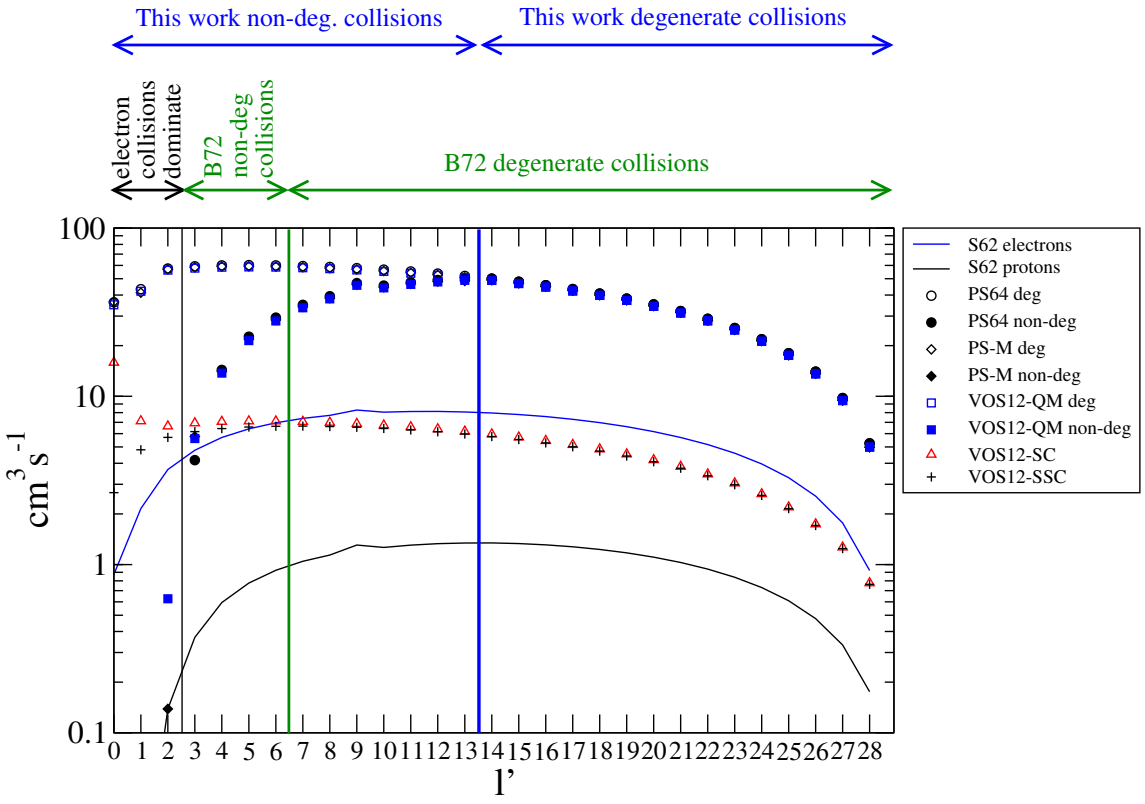

Figure 1. Comparison of l-mixing collisional rate coefficients for H^++He($n = 30$) singlet collisions for $\Delta l = l - l' = 1$ as a function of the final subshell l' for $T = 10^4$K and $n_H = 10^4 cm^{-3}$. The B72 criterion from (4) is satisfied usually for $l > 7$ ($l' > 6$) (see the text). In the graph are shown also the limits for electron collisions dominating over protons, and the point where cut-offs from equations (1) and (3) are equal. Blue solid line: S62 electron collisions; black solid line: S62 proton collisions; open black circles: original PS64 degenerate levels calculations; full black circles: original PS64 calculations using non-degenerate cut-off; open black diamonds: PS-M degenerate levels calculations; full black diamonds: PS-M calculations using non-degenerate cut-off; open blue squares: VOS12-QM degenerate levels calculations; full blue squares: VOS12-QM calculations using non-degenerate cut-off; open red triangles: VOS12-SC; black + symbols: VOS12-SCC.

$U_m = U_c$ corresponds to using the Debye cut-off at all energies while $E_1(U_c \to \infty) \to 0$ corresponds to using the lifetime/splitting one. PS64 made the additional assumption $E_{min} \ll k_B T$ and expanded the exponential factors to leading order. We do not.

This rate coefficient (14) neglects the contribution from cross sections with $E < E_{min}$, i.e. $R_c < R_1$ by definition. This was reasonable for PS64 to do since $P = 1/2$ there. Now that we have a more reasonable representation of $P(R < R_1)$ it makes sense to include it. Then, the cross sections arise only from integration over probabilities given by (9), with R_1 replaced[2] by R_c. Then,

$$\sigma_{ji}(E \leqslant E_{min}) = \frac{2}{3}\pi P_1 R_c^2 . \qquad (15)$$

This is readily convolved with a Maxwellian distribution to give the *additional* contribution to the rate coefficient, given by (14), from $0 \leqslant E \leqslant E_{min}$:

$$q_{ji}(E \leqslant E_{min}) = \frac{a_0^3}{\tau_0 \omega_l}\left(\frac{\pi M I_H}{k_B T}\right)^{\frac{1}{2}} D_{ji} \times \frac{2}{3}\left[2 - 2e^{-\overline{U}_m}(1 + \overline{U}_m + \frac{1}{2}\overline{U}_m^2)\right]/\overline{U}_m^2 . \qquad (16)$$

[2] Use of R_1 here leads to $P(R) \to 0$ as $E \to 0$ (since $R_1 \to \infty$ then) which is not born out by the QM $P(R)$.

We note that the cut-off assumed here is the energy dependent lifetime/splitting one. In the highly unlikely case that

$$U_c < \overline{U}_m \qquad \text{and, hence,} \qquad U_c < U_m , \qquad (17)$$

then the convolution integral is easily split into two again. However, a search of the parameter space has not given a case where the condition (17) was satisfied. The contribution from equation (16) varies, being typically $\sim 5\%$ of (14), and thus is important for accurate calculations. At very low temperatures and very high densities, $T \lesssim 100$ K and $n_H \gtrsim 10^{10} cm^{-3}$ (these values depend on the energy difference of the transition and the lifetime of the initial state), the contribution from equation (16) might be larger than equation (14), which is the 'main' term. In that case, more accurate approaches may be necessary to be taken in account for the calculation of the probabilities.

Following a widespread comparison of PS-M and QM results on H, we take $P_l = 1/4$, corresponding to a constant 'branching ratio' of $1/2$ in that picture — see Appendix A. But, use of an l-dependent branching ratio gives only marginally worse results overall at low-l. Note, this validates PS64's final choice of $P = \sum_{j \neq i} P_{ji} = 1/2$ rather than $P = P_{ji}$. A comparison between selected l-changing rate coefficients is given in Table 1.

The SC rate coefficients do not have imposed cut-offs and do not depend on density. They depend linearly on temperature. The Debye cut-off makes the QM rate coefficients decrease as the density increases (as seen at high l), and they have a more complicated

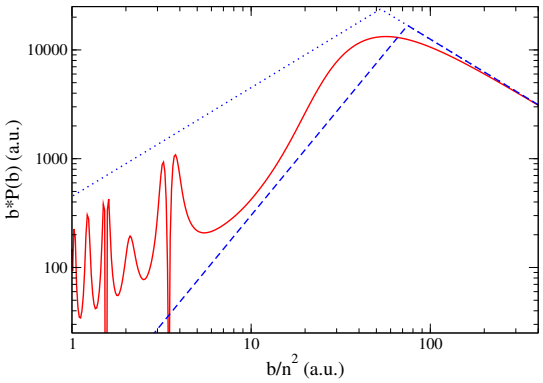

Figure 2. Probability times the impact parameter versus scaled impact parameter for H^++He($n = 30$; $l = 29 \rightarrow 28$), at $v = 0.25/n$. Solid line, VOS12-QM; dotted line, PS64 ($P_l = 1/2$) ; dashed line, modified PS-M probabilities from equation (9), and (7).

temperature dependence due to structure within the probability distribution. The ratio between the PS-M rate coefficients and the 'standard' PS64 ones increases for higher densities and lower temperatures but this difference is only a few percent, except for low l and low temperatures, where the energy separation of the l levels makes the large cut-off R_c comparable to the small cut-off R_1. As expected, the modification of the small impact parameter probability causes PS-M to be in much better agreement with VOS12-QM rate coefficients for all temperatures and densities, although there are still large differences at $T = 10^2 K$ and $l = 4 \rightarrow l' = 3$ where the PS-M rate coefficients overestimate the VOS12-QM ones by a factor ~ 10. These differences, shown in Table 1, could produce a significant effect on line intensities as seen in Fig. 3.

3 CLOUDY SIMULATIONS

The impact of these changes in the l subshell collisional data on He I recombination line emission was tested in Cloudy using a model very similar to the one used in P1 for H I spectra. Line emissivities applying both the QM and SC formalisms are compared to estimate the uncertainty created by differences in the theories considered here.

3.1 Description of the model for He

We use the development version of Cloudy, the spectral simulation code last described by Ferland et al. (2013). The results presented in this paper come from the branch Hlike_HS87 at revision r11113.

As in the H-only case (P1), a single layer of gas has been considered and emissivities from recombination lines calculated. A cosmic helium abundance, He/H =0.1, was assumed. The cloud is radiated by a narrow band of radiation, a 'laser', centered at 2 Ryd, with an ionization parameter of U = 0.1 (Osterbrock & Ferland 2006). The state of the emitting gas in these conditions resembles that in H II regions, observationally relevant for the determination of He abundances (Izotov et al. 2014). In this calculation we set the code to ignore internal excitations that might have been produced by the incident radiation field. A constant gas kinetic temperature of 1×10^4 K is assumed. As in the previous paper, we assume 'Case B' (Baker & Menzel 1938), where Lyman lines with upper shell $n > 2$ are assumed to scatter often enough to be degraded into Balmer lines and Lyα. The hydrogen density is varied over a wide range and the electron density is calculated self-consistently. The latter is approximately 10% greater than the hydrogen density since He is singly ionized. The atomic data used for He and H emission, except for l-changing collisions, are the 'standard' set of data that has been described in previous works (Porter et al. 2005).

The hydrogen density ranges from 10 cm^{-3} to 10^{10} cm^{-3}, a range of densities large enough to cover diverse astrophysical environments from the interstellar medium to quasars. As in the case of hydrogen, n-shell states can be treated as 'resolved', where all l subshells are modeled separately, or 'collapsed' where the l subshell population is statistically distributed. The chosen maximum principal quantum number for resolved levels, n_r, is density dependent (PS64), with $n_r \sim 60$ at the lowest density and $n_r = 20$ at the highest density.

A set of 411 of the brightest He I lines has been selected in a range from 2000Å to 30μm covering most of the spectral range of today's observations. These are both singlet and triplet transitions, where the upper levels have principal quantum numbers between $n = 3$ and $n = 36$, and the lower levels have n between 2 and 8.

3.2 Results

As in P1, a comparison of line emissivities will show the behaviour of different l-changing theories. Predicted emissivities, normalized to the PS-M theory, are presented in Fig. 3 for each of the theories described in P1 and discussed here. Density is increasing from upper left to bottom right.

As in the case of H I, changes in the l-changing data have little impact at very low densities, where radiative decays are much faster than l-changing collisions. The predictions do change between densities of $n_H = 10^4 - 10^{10}$cm^{-3}, where l-mixing processes compete with radiative decay. At the highest densities, collisions start to dominate over radiative processes and the l subshells come into LTE. Differences in the rate coefficients result in deviations up to $\sim 7\%$ in many lines. Paschen ($\lambda \sim 9000$ Å) and Brackett ($\lambda \sim 15000$ Å) series are clearly visible. Note that $l < 3$ collisions are considered to be dominated by electron-impact and so no differences are expected for the Balmer series except as a result of cascading from higher n. We find the largest effect at densities around $n_H = 10^5 - 10^9$cm^{-3}. For all transitions, the larger the upper level quantum number n is, the more l subshells are available for redistribution and differences in the l-mixing collisions data become more important. As in the case of H I, the two simulations based on QM calculations (PS-M and VOS12-QM) agree much more closely with each other for all densities considered than with the two based on SC data (VOS12-SC and VOS12-SSC). The latter have emissivities that are different from PS-M, particularly for lines where the upper level has a high principal quantum number n. This effect is more pronounced for densities of $n_H = 10^7$ cm^{-3} and $n_H = 10^8$ cm^{-3} where at high n levels, collisional effects are strong and comparable with radiative decay. Therefore, differences in the l-changing collisional rates have a larger impact at these densities. This also happens on a smaller scale at the immediately lower densities of $n_H = 10^5$ cm^{-3} and $n_H = 10^6$ cm^{-3}, where the smaller collisional rates produced by the SC approaches lead to noticeable differences in emissivities.

3.2.1 *Impact on observed He I low n lines*

We have also examined the impact of the various l-changing theories on the emissivities of the most commonly observed lines at

Table 1. Comparison of rate coefficients (cm^3s^{-1}) from the different theoretical SC and QM methods for $n = 30$ and low- and high-l for different temperatures and densities. PS64: 'standard' PS64 from equation (A4); PS-M: equation (14); VOS12-QM: QM method from equation (2) in Vrinceanu et al. (2012); VOS12-SC: SC method from equation (6) in Vrinceanu et al. (2012); VOS12-SSC: Simplified SC method from equation (9) in Vrinceanu et al. (2012). The relatively large energy separation of the $l = 4 \rightarrow l' = 3$ transition leads to $R_c < R_1$ at $T = 100$K and the 'standard' PS64 formula gives a negative result.

		$n_H = 10^2 cm^{-3}$			$n_H = 10^4 cm^{-3}$			$n_H = 10^6 cm^{-3}$		
		$T_H = 10^2$K	$T_H = 10^4$K	$T_H = 10^6$K	$T_H = 10^2$K	$T_H = 10^4$K	$T_H = 10^6$K	$T_H = 10^2$K	$T_H = 10^4$K	$T_H = 10^6$K
$l = 4 \rightarrow l' = 3$	VOS12-QM	1.66e-3	5.61e+0	3.51e+0	1.66e-3	5.61e+0	3.51e+0	1.66e-3	5.61e+0	3.51e+0
	PS64	—	4.18e+0	3.65e+0	—	4.18e+0	3.65e+0	—	4.18e+0	3.65e+0
	PS-M	2.00e-2	5.77e+0	3.57e+0	2.00e-2	5.77e+0	3.57e+0	2.00e-2	5.77e+0	3.57e+0
	VOS12-SC	6.94e+1	6.94e+0	6.94e-1	6.94e+1	6.94e+0	6.94e-1	6.94e+1	6.94e+0	6.94e-1
	VOS12-SSC	6.17e+1	6.17e+0	6.17e-1	6.17e+1	6.17e+0	6.17e-1	6.17e+1	6.17e+0	6.17e-1
$l = 29 \rightarrow l' = 28$	VOS12-QM	3.80e+1	6.18e+0	8.55e-1	2.61e+1	4.99e+0	7.35e-1	1.42e+1	3.80e+0	6.16e-1
	PS64	4.06e+1	6.44e+0	8.81e-1	2.87e+1	5.25e+0	7.61e-1	1.68e+1	4.06e+0	6.42e-1
	PS-M	3.80e+1	6.18e+0	8.54e-1	2.60e+1	4.99e+0	7.35e-1	1.41e+1	3.79e+0	6.16e-1
	VOS12-SC	7.76e+0	7.76e-1	7.76e-2	7.76e+0	7.76e-1	7.76e-2	7.76e+0	7.76e-1	7.76e-2
	VOS12-SSC	7.63e+0	7.63e-1	7.63e-2	7.63e+0	7.63e-1	7.63e-2	7.63e+0	7.63e-1	7.63e-2

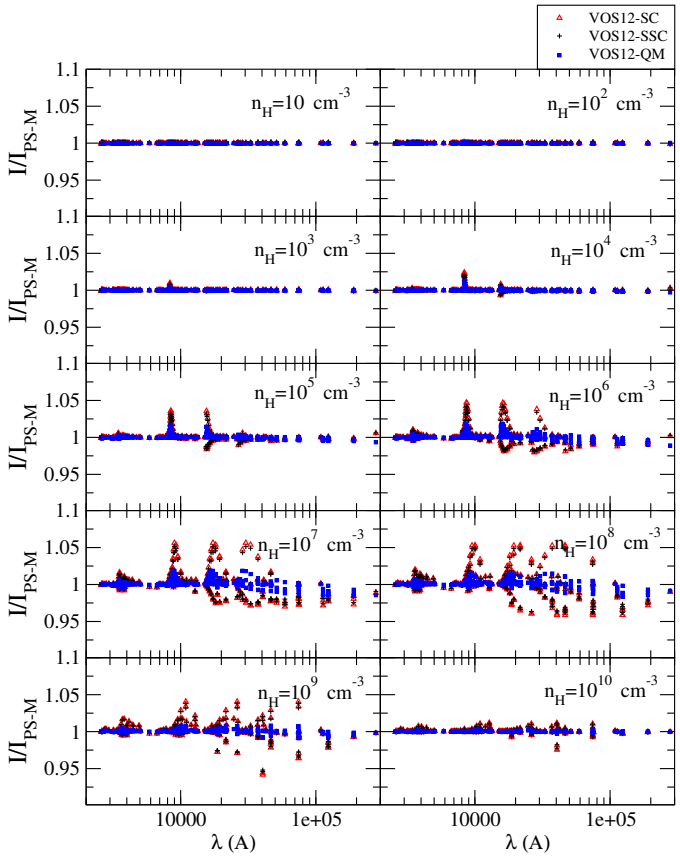

Figure 3. Ratios of He I lines for Cloudy simulations using the different data sets considered in this work with respect to the PS-M approach, for $T = 10^4$K.

visible wavelengths. These lines have relatively small upper n, typically 3 or 4, therefore low-l dipole transitions, with these being dominated by *ns*, *np*, and *nd* subshells, so it is expected that the various l-changing heavy impact collisions will only affect these lines through cascades from higher levels which are affected. Table 2 lists emissivities of some important lines normalized to PS-M. These are given as a function of temperature and density for the different cases considered here. For these representative low-lying lines, l-changing collisions have a greater effect at low temperatures where the Stark mixing from the projectile is more effective. There are also larger differences at high densities, where collisional processes dominate over radiative. The differences between VOS12-QM and PS-M are generally smaller than 1%. However, at low temperatures the 4471.49Å predicted intensities disagree by ∼2%, presumably as a consequence of the cumulative effects of the differences in rates seen in Table 1. The SC results can disagree by up to ∼10% for 4471.49Å line and by up to ∼5% for 7065.22Å 5875.64Å and 6678.15Å lines, for $T = 100K$ and $n_H = 10^4$. These

differences can increase by up to ∼14%, ∼11%, ∼10% and ∼10%, respectively, for the extreme case of $n_{\rm H} = 10^6{\rm cm}^{-3}$ and $T = 100K$. None of the lines in Table 2 correspond to a transition with $l \geqslant 3$, so l-changing transitions are dominated by electron collisions. However, the upper levels of the first three lines in table 2 arise from $l = 2$ which receives electrons for $\Delta l = 1$ transitions from $l = 3$ subshells that are partially populated by Stark effect l-changing mechanisms. Cascade effects from higher l are important for the 1s3s ^{1}S – 1s2p ^{1}P transition at 7281.35Å. The 10830.31Å intrashell triplet-triplet transition 1s2s ^{3}S – 1s2p ^{3}P is less likely to be affected by differences in l-changing collisions since the emission line is mainly produced by electron collisions from the metastable lower level, and cascade effects make only a small contribution.

3.2.2 *Effect of multipole l-changing*

Multipolar l-changing collisions strengthen l-mixing at high n and can have an effect on emissivities. PS64 assumed multipole ($\Delta l > 1$) l-changing rates to be negligible compared with dipole ones. VOS12 calculate the multipole dependence as $(\Delta l)^{-3}$ for SC calculations. The results for the emissivities presented in Fig. 3 and Table 2 are obtained considering all possible multipolar l-changing transitions for VOS12-QM, VOS12-SC and VOS12-SSC results, while only dipole transitions are allowed by PS64 and PS-M. We have done that in order to get the best prediction that each of the approaches can provide.

The effect of multipolar transitions can be quantified by progressively switching-off $\Delta l > 1, 2, 3$, l-changing transitions in our calculations at different densities. We have found these effects negligible at most densities except for intermediate densities ($n_{\rm H} = 10^5 - 10^6{\rm cm}^{-3}$), where differences in emissivities are up to $\sim 2\%$ when these transitions are included in VOS12-QM rates for $n_{\rm H} = 10^6{\rm cm}^{-3}$. In Fig. 4, the multipole effects constitute the main contribution to the disagreement between VOS12-QM and PS-M results at this density. Quadrupolar transitions contribute up to $\sim 50\%$ of the total difference of the emissivities with PS-M results. Multipoles have a similar contribution to both Paschen and Bracket lines and can also influence Balmer lines by cascade effects (note that $l \rightarrow l' \leqslant 2$ transitions are dominated by electron impact and calculated in a similar way in both cases). Similar effects are seen for SC calculations. The overall magnitude of these effects is significantly smaller than for the SC/QM differences which are the focus of the present paper, but are still at a level which would have a significant impact on the determination of cosmological abundances. Improving the accuracy of these predictions in a computationally efficient manner will be the subject of future work.

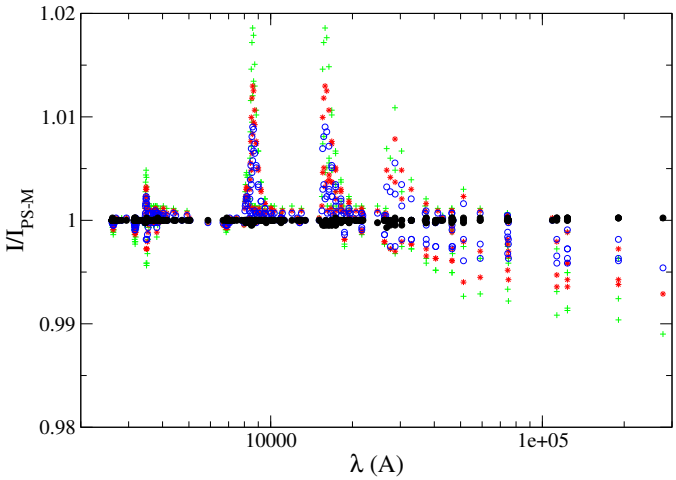

Figure 4. Ratios of He I lines for VOS12-QM to PS-M (dipole) data from Cloudy simulations including different multipolar l-changing transitions at $T = 10^4$K and $n_{\rm H} = 10^6{\rm cm}^{-3}$. Black filled circles: $\Delta l = 1$; blue open circles: $\Delta l < 3$; red stars: $\Delta l < 4$; green crosses: all multipoles.

4 CONCLUSIONS

We have applied the different theories of l-changing collisions to the more complicated case of He. In summary:

- We have improved the accuracy of the PS64 Bethe approximation by modifying the probability at small impact parameters so it resembles better the pure QM calculations of VOS12. We have not followed the PS64 assumption of $E \gg E_{\rm min}(R_1 \ll R_{\rm c})$. The contribution from small energies to the integration, which was neglected by PS64, is taken into account and changes the final rate coefficients by about 5%. We call this improved theory PS-M.
- Cut-offs are important for impact parameter theory. These highly accurate results can be applied in the non-degenerate case where they are integrated to different large impact parameter cut-offs due the energy differences between intrashell l-subshells. The criteria to decide when to apply degenerate or non-degenerate cut-offs has been refined to obtain a continuous variation of the rate coefficients as a function of l.
- We have compared our improved results with the more accurate VOS12-QM results and with the SC theories (which do not account for non-degeneracy within l subshells). The new PS-M based emissivities are in very good agreement with the pure QM VOS12-QM results and both disagree with SC predictions. Cloudy simulations show that the He I line emissivities predicted by these different l-changing theories change by up to 10%. However, emissivity differences of ∼2% remain between the VOS12-QM theory and the PS-M model at intermediate densities $10^4 - 10^8{\rm cm}^{-3}$, where radiative and collisional processes compete. Most of this difference can be attributed to non-dipole l-changing collisions which the PS-M approach neglects. This should be taken in account when testing Big Bang nucleosynthesis models, which require a precision better that 1%.

The main result of this work is an improved l-changing theory, PS-M, which is highly accurate at nearly all densities and temperatures and is computationally fast and easy to implement. We recommend using PS-M for $l \geqslant 3$ l-changing collisions rates in order to obtain good accuracy He I spectral intensities. However, it must be noted that no observational or experimental measurement has been done up to date that supports any of the data sets over the other. Our recommendations are based uniquely on theoretical considerations on the long impact parameter probabilities differences described in P1. Only observations or experiment can definitely set the validity of one of the calculations over the others.

The PSM approach will be the default in the next release of Cloudy for this type of collisions. However, we also provide the more precise VOS12-QM method, which is computationally more expensive, to allow testing of the various methods and for when even higher accuracy results are needed.

Table 2. Some representative emissivities for the He I spectrum, normalized to PS-M results, at various densities and temperatures. The VOS12 labels are as in table 1.

		$n_{\rm H}=10^2{\rm cm}^{-3}$			$n_{\rm H}=10^4{\rm cm}^{-3}$			$n_{\rm H}=10^6{\rm cm}^{-3}$		
		$T_H=10^2$K	$T_H=10^4$K	$T_H=10^6$K	$T_H=10^2$K	$T_H=10^4$K	$T_H=10^6$K	$T_H=10^2$K	$T_H=10^4$K	$T_H=10^6$K
4471.49 Å	VOS12-QM	1.007	1.000	1.000	1.020	1.000	1.000	1.010	1.001	1.001
	VOS12-SC	1.025	1.000	1.000	1.105	1.000	0.999	1.138	1.001	0.997
1s4d ^{3}D – 1s2p ^{3}P	VOS12-SSC	1.024	1.000	1.000	1.103	1.000	0.999	1.134	1.001	0.997
5875.64 Å	VOS12-QM	1.001	1.000	1.000	1.003	1.000	1.000	0.999	1.000	1.000
	VOS12-SC	0.992	1.000	1.000	0.959	1.000	1.000	0.900	0.998	1.000
1s3d ^{3}D – 1s2p ^{3}P	VOS12-SSC	0.992	1.000	1.000	0.961	1.000	1.000	0.902	0.999	1.000
6678.15 Å	VOS12-QM	0.998	1.000	1.000	0.997	1.000	1.000	0.998	1.000	1.000
	VOS12-SC	0.989	1.000	1.000	0.951	1.000	1.000	0.901	0.998	1.001
1s3d ^{1}D – 1s2p ^{1}P	VOS12-SSC	0.990	1.000	1.000	0.952	1.000	1.000	0.903	0.998	1.001
7065.22 Å	VOS12-QM	1.000	1.000	1.000	1.001	1.000	1.000	1.003	1.000	1.000
	VOS12-SC	1.009	1.000	1.000	1.055	1.000	1.000	1.111	1.000	1.000
1s3s ^{3}S – 1s2p ^{3}P	VOS12-SSC	1.009	1.000	1.000	1.053	1.000	1.000	1.109	1.000	1.000
7281.35 Å	VOS12-QM	0.998	1.000	1.000	0.992	1.000	1.000	0.997	1.000	1.000
	VOS12-SC	1.002	1.000	1.000	1.012	1.000	1.000	1.059	1.000	1.000
1s3s ^{1}S – 1s2p ^{1}P	VOS12-SSC	1.002	1.000	1.000	1.011	1.000	1.000	1.057	1.000	1.000
10830.31 Å	VOS12-QM	1.002	1.000	1.000	1.005	1.000	1.000	1.002	1.000	1.000
	VOS12-SC	1.000	1.000	1.000	1.003	1.000	1.000	0.992	1.000	1.000
1s2s ^{3}S – 1s2p ^{3}P	VOS12-SSC	1.001	1.000	1.000	1.003	1.000	1.000	0.992	1.000	1.000

5 ACKNOWLEDGMENTS

We acknowledge support by NSF (1108928, 1109061, and 1412155), NASA (10-ATP10-0053, 10-ADAP10-0073, NNX12AH73G, and ATP13-0153), and STScI (HST-AR- 13245, GO-12560, HST-GO-12309, GO-13310.002-A, HST-AR-13914, and HST-AR-14286.001). MC has been supported by STScI (HST-AR-14286.001-A). PvH was funded by the Belgian Science Policy Office under contract no. BR/154/PI/MOLPLAN.

REFERENCES

Baker J. G., Menzel D. H., 1938, ApJ, 88, 52
Benjamin R. A., Skillman E. D., Smits D. P., 1999, ApJ, 514, 307
Brocklehurst M., 1972, MNRAS, 157, 211
Ferland G. J., Porter R. L., van Hoof P. A. M., Williams R. J. R., Abel N. P., Lykins M. L., Shaw G., Henney W. J., Stancil P. C., 2013, Revista Mexicana de Astronomia y Astrofisica, 49, 137
Guzmán F., Badnell N. R., Williams R. J. R., van Hoof P. A. M., Chatzikos M., Ferland G. J., 2016, MNRAS, 459, 3498
Hummer D. G., Storey P. J., 1987, MNRAS, 224, 801
Izotov Y. I., Thuan T. X., Guseva N. G., 2014, Monthly Notices of the Royal Astronomical Society, 445, 778
Izotov Y. I., Thuan T. X., Stasiska G., 2007, The Astrophysical Journal, 662, 15
Olive K. A., Steigman G., Walker T. P., 2000, Phys. Rep., 333, 389
Osterbrock D. E., Ferland G. J., 2006, Astrophysics of gaseous nebulae and active galactic nuclei, 2nd. ed.. Sausalito, CA: University Science Books
Pengelly R. M., Seaton M. J., 1964, MNRAS, 127, 165
Porter R. L., Bauman R. P., Ferland G. J., MacAdam K. B., 2005, ApJ, 622, L73
Porter R. L., Ferland G. J., MacAdam K. B., Storey P. J., 2009, Monthly Notices of the Royal Astronomical Society: Letters, 393, L36
Porter R. L., Ferland G. J., Storey P. J., Detisch M. J., 2012, MNRAS, 425, L28
Seaton M. J., 1962, Proceedings of the Physical Society, 79, 1105
Storey P. J., Hummer D. G., 1995, MNRAS, 272, 41
Summers H. P., 1977, MNRAS, 178, 101
Vrinceanu D., Flannery M. R., 2001a, Phys. Rev. A, 63, 032701
Vrinceanu D., Flannery M. R., 2001b, Journal of Physics B Atomic Molecular Physics, 34, L1
Vrinceanu D., Onofrio R., Sadeghpour H. R., 2012, ApJ, 747, 56

This paper has been typeset from a TEX/ LATEX file prepared by the author.

APPENDIX A: RESOLVED VS UNRESOLVED FINAL-STATES AND RECIPROCITY.

The Pengelly & Seaton (1964) formula is for an unresolved, by final state, rate coefficient q_{nl} for $nl \to nl'$ summed-over $l' = l \pm 1$. In general, we require a final-state resolved expression.

Define P_1 of Section 2.3 by

$$P_1 = \frac{1}{2} B_{ji} \tag{A1}$$

where the branching ratio B_{ji} is given by

$$B_{ji} = \frac{D_{ji}}{w_l D_{nl}} \tag{A2}$$

and D_{nl}, the quantity used by PS64, is given by

$$D_{nl} \equiv \sum_{l'=l\pm1} \frac{1}{\omega_l} D_{ji} = \frac{Z^2}{z^2} 6n^2(n^2 - l^2 - l - 1)\,. \tag{A3}$$

This leads to the final-state resolved form of the PS64 formula

$$q_{ji} = 9.93\times10^{-6}\mathrm{cm^3 s^{-1}}\left(\frac{\mu}{m_e}\right)^{1/2} \times\frac{D_{ji}}{\omega_l T^{1/2}}\left[11.54+\log_{10}\left(\frac{Tm_e}{D_{nl}\mu}\right)+2\log_{10}(R_\mathrm{c})\right], \quad \text{(A4)}$$

as used by Cloudy (Ferland et al. 2013), Hummer & Storey (1987) and Summers (1977). The sum over the final l' then recovers the original PS64 unresolved value. The unresolved PS-M result for arbitrary P_l is obtained simply by summing-over $l' = l \pm 1$. In general, there is no corresponding closed-expression for it, or need for one.

An issue which affects all forms of the Pengelly and Seaton method is the lack of reciprocity because of the D_{nl} factor in the $\log_{10}$ term. The standard approach, as used by Cloudy, is to calculate all rate coefficients in one direction ($l \rightarrow l-1$, say) and obtain the rate coefficient for the reverse direction using the principle of detailed balance, viz. $(2l-1)q_{nl-1\rightarrow nl} = (2l+1)q_{nl\rightarrow l-1}$ (for $\Delta E_{ll'} \approx 0$). In general (Summers (1977)), results are not sensitive to the $\log_{10}$ term and, even if they are, the *ad hoc* nature of the original definition of R_1 means that the treatment is unreliable here.

Comparison of our PS-M $s-p$ rate coefficients calculated in both directions with the QM result shows that the $p \rightarrow s$ result lies above the QM one while the $s \rightarrow p$ lies below, by almost the same amount but a little larger. The difference depends strongly on the value of R_c compared to R_1 but only exceeds $\sim 10\%$ in extreme cases where the plasma screening is about to delocalise the state. The difference rapidly decreases with increasing l. For helium, we do not use any form of Pengelly and Seaton for $l = 0-2$.